Frontiers in Heat and Mass Transfer

Tech Science Press

DOI: 10.32604/fhmt.2023.042639 Published Online: 28 September 2023

ARTICLE

Cross Flow Characteristics and Heat Transfer of Staggered Tubes Bundle: A Numerical Study

Husam Rashid Hudear* **and Saad Najeeb Shehab**

Department of Mechanical Engineering, College of Engineering, Mustansiriyah University, Baghdad, Iraq

*Corresponding Author: Husam Rashid Hudear. Email: ehma048@uomustansiriyah.edu.com

Received: 07 June 2023 Accepted: 25 July 2023

ABSTRACT

This paper presents a numerical emulation study of heat transmission through tube banks in three-dimensions. Staggered configuration is displayed by fluid dynamics using computer programs (CFD) software (ANSYS fluent). The computer model is used to predict the values of the Nusselt number when changing the values of heat flux and longitudinal pitch. The longitudinal pitch (SL/D) of 1.3, 1.8, and 2.4 mm. The transverse pitch (ST/D) of 1.5 mm, and also considered Reynolds numbers 10000, 13000, 17000, and 190000. The staggered configuration of the tube bundle is demonstrated to investigate the impact of this arrangement on the heat transmission rate from the tubes. The gotten results indicate that the rate of heat transmission increases with decreases in the longitudinal spacing (SL). As the longitudinal spacing (SL) increases to about 44% the Nusselt number is slightly decreased by about 9%. The coefficient of heat transmission, Nusselt number, and the heat transmission data obtained from (CFD) Compared to previous research results, there is a decent agreement originating after comparison.

KEYWORDS

Tube bundle; numerical study; longitudinal pitch; cross-flow; staggered

Nomenclature

C_P	Specific heat (J/Kg.K)
V_{max}	Maximum velocity (m/s)
V_i	Inlet velocity (m/s)
S_D	Diagonal spacing (m)
N_T	Number of tubes in column
D	Diameter of tubes (m)
$\overline{h}$	Average heat transmission coefficient (W/m^2.K)
K	Thermal conductivity (W/m.K)
L	Length of tubes (m)
N	Number of tubes
$\overline{Nu}$	Average nusselt number
Q	Heat transmission rate (W)
Re	Reynolds number

$T_{S,a}$	Average surface temperature (K)
S_L	Longitudinal pitch (m)
S_T	Transverse pitch (m)
T_O	Outlet air temperature (K)
T_i	Inlet air temperature (K)
ΔT_{lm}	Log mean temperature (K)
G_k	Generation of turbulent kinetic energy due to mean velocity
G_b	Generation of turbulent kinetic energy due to buoyancy
Y_M	Fluctuating dilatation in compressible turbulence to the overall dissipation rate
α_k *and* α_ε	Represents the inverse of the effective Prandtl number for (k and ε), respectively
S_k *and* S_ε	The user-defined source term
μ_t	Turbulent viscocity
j	Heat transfer factor

Subscripts

i	Inlet
f	Fluid
o	Outlet
p	Pressure (N/m^2)
T	Temperature (K)
S	Tube surface

Greek symbols

ρ	Density (Kg/m^2)
α	Thermal diffusivity (m^2/s)
υ	Kinematic viscosity (Pa.s)

1 Introduction

The rate of heat transmission and fluid flow in the bundle of tubes exemplifies several industrial important operations. The bank of tubes is typically used in the cross-flow of heat exchangers. The design relies on empirical relationships between pressure drop with the amount of heat transfer. The heat exchangers and tubes bundle in cross-flow are of large workable interest in several chemical and thermal engineering applications. The bank of tubes uses in several important industrial operations, like thermal power stations, conditioning systems, and heating systems. Several tube designs may be achieved for efficient heat transmission between fluids. Tube bundles are typically coordinated in a staggered or an in-line arrangement [1–5].

Many studies have investigated the improvement of heat transfer through a bundle of tubes. Tahseen et al. [6] studied heat transfer by forced convection on a two-dimension staggered bank of tubes for cross-flow steady-state, incompressible conditions using the FDM procedure across a laminar flow field at the tube banks. The steady heat flux was placed on the surface of the tubes with a tube diameter of 15 mm, and the number of tubes was 10. The ratio of longitudinal pitch to diameter is 1.25, 1.5, and 2. Reynold's number range is 50 to 250. They discovered that the heat transmission rate increased with a decreased longitudinal pitch. Mangrulkar et al. [7] examined the numerical analysis of friction factor and heat transmission properties to cam-shaped an in-line tube bundle in cross-flow utilizing the ANSYS Fluent code (14.5) computational fluid dynamic (CFD). The Reynold

number ranges from 11500 to 42500. The number of tubes was 16 and the diameter was 22.45 mm. The longitudinal and transverse pitch ratios are 1.5, and 1.25, respectively. The numerical simulation results show that the cam-shaped tube banks outperform the circular tubes in terms of thermal performance. Because the friction factor is lowered by 85–89% when compared to circular tubes, heat transmission by friction factor (Nu/f) is boosted by 5 times. Saraireh et al. [8] searched the heat transmission for an in-line and staggered bank of tubes using (CFD) code ANSYS Fluent software. The shape of the tube that was used is oval with a large diameter of 18.5 mm, and a small diameter of 10 mm, and the number of tubes was 16. The longitudinal pitch is 40 mm, and the transverse pitch is 42 mm. The Reynold number changed from 400 to 650. The heat flux varies from 1000 to 3500 W/m^2. They find that the average value of the Nusselt number increased with increasing the velocity of the fluid and walls heat flux. Refaey et al. [9] studied convective heat transmission from disorderly flow through the staggered banks of tubes and was examined numerically. They used (CFD) program ANSYS Fluent with Reynold number varies from 5000 to 50000. At transverse pitch with ratio (S_T/D) = 1.25, the longitudinal pitch ratio (S_L/D) changed from 1.25 to 3. The number of tubes was 25, and the diameter was 10 mm. The results for the plane tube bank demonstrate that heat transmission rises as the longitudinal ratio lowers. Furthermore, to get the greatest heat transmission, the diameter of the plane tube should be small. Numerical investigation of the effect of changing tube pitches on heat and flow characteristics from tube bundles in cross flow within the Reynolds number limit from 7381 to 22214 [10]. They used ANSYS Fluent. The diameter of the tube was 15.88 mm, and the number of tubes is 27. They found that tube bundles with decreasing pitches performed better in terms of heat transmission, but those with rising pitches had lower levels of friction. Deeb et al. [11] studied the heat dissipation and friction factor of staggered tube bundle in cross-flow. They used (CFD) ANSYS Fluent software with Reynold numbers 1800 to 18700. The diameter of the equivalent circular tube is 22.44 mm. The tube with an oval design offers better thermal efficiency, according to the results. Tassone et al. [12] performed a simulation for turbulence heat transmission for low-Pr fluid in the tube bundle. They used (CFD) fluent ANSYS coding considering heavy liquid metals (HLM) as the fluid domain. The calculation of the heat transmission at P_r (Prandtl number) = 0.85 and the ratio $\left(\frac{S_T}{D}\right) < 1.25$ for staggered tube banks. The tube diameter was 16 mm. The results show a poor heat transmission rate. In a heated tube bank, it was studied how to get the reference temperature for a convective heat transmission coefficient [13]. They used (CFD) package ANSYS Fluent software with Reynold numbers range 1000 to 10000, $S_L = S_T = 40$ mm. The number of tubes was 40 and the tube diameter was 20 mm. The results revealed that a staggered configuration increased temperature more than an in-line arrangement. Ariansyah et al. [14] investigated the effect of gap ratio on flow characteristics and heat transmission in staggered tube bundles: A numerical investigation. They used computational fluid dynamics (CFD) with a velocity of 7.07 m/s.The tube diameter was 25.4 mm. The transverse pitch varies by 1.7, 2, 2.7, and 3.2 mm. They concluded that the results showed a smaller gap ratio, produced a lower outlet temperature and the greatest heat transmission but obtained a bigger measured pressure decrease [15–19].

Inside this investigation, a bank of copper tubes that are submerged in cross-flowing air at room temperature serves as the model system. The purpose of the study is to investigate the heat-transmission enhancement of a 3D tube bundle with various configurations by studying the effects of the tube pitch at different heat fluxes. The sample is employed to forecast the average Nusselt number and the rate of heat transmission caused by convective heat.

2 Methodology

The three-dimensional, staggered tube bank problem under study has a tube diameter of 19 mm, a tube length of 270 mm (Table 1), and a longitudinal pitch (SL) of 25, 35, and 45 mm. The transverse pitch is 28 mm. The transport equations of the conservation of energy, continuity, and momentum equations serve as the fully expanded form of 3D coordinates [20–24]. Using three-dimensional formulas in Cartesian vector notation for steady-state incompressible flow fully developed. The physical system that was created for this investigation is shown in Figs. 1a–1d.

Table 1: Physical characteristics and tube dimensions

No.	Tube parameters	Quantity
1	Tube material	Copper
2	Thermal conductivity	387.6 W/m.K
3	Density	8978 Kg/m^3
4	Tube diameter	19 mm
5	Tube length	270 mm
6	Tube thickness	0.8 mm
7	Tubes number	15

Energy:

$$u\frac{\partial T}{\partial x}+v\frac{\partial T}{\partial y}+w\frac{\partial T}{\partial z}=\alpha\left(\frac{\partial^2 T}{\partial x^2}+\frac{\partial^2 T}{\partial y^2}+\frac{\partial^2 T}{\partial z^2}\right) \tag{1}$$

Continuity:

$$\frac{\partial \mathrm{u}}{\partial \mathrm{x}}+\frac{\partial \mathrm{v}}{\partial \mathrm{y}}+\frac{\partial \mathrm{w}}{\partial \mathrm{z}}=0 \tag{2}$$

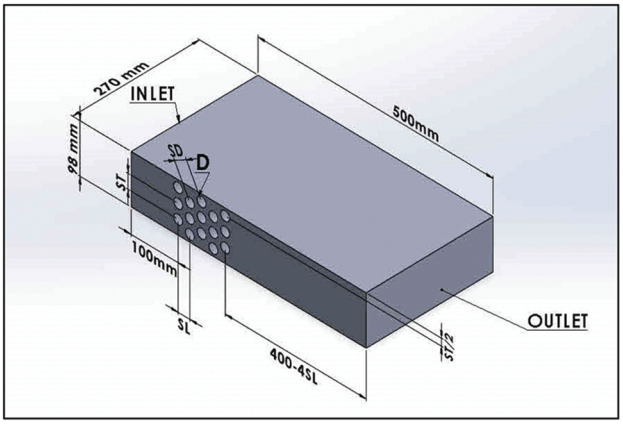

Figure 1a: The distribution of pipes, longitudinal pitch, transverse pitch, and air inlet and outlet

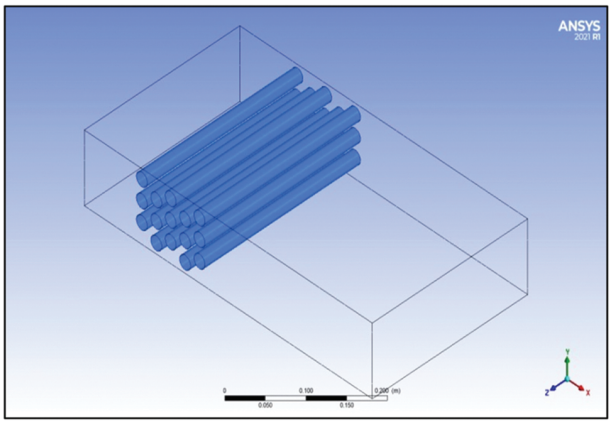

Figure 1b: The three-dimensional distribution of the tube bundle inside the duct with a longitudinal pitch of 25 mm

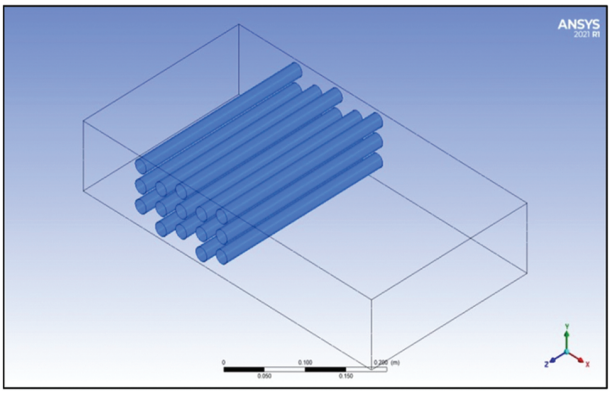

Figure 1c: The three-dimensional distribution of the tube bundle inside the duct with a longitudinal pitch of 35 mm

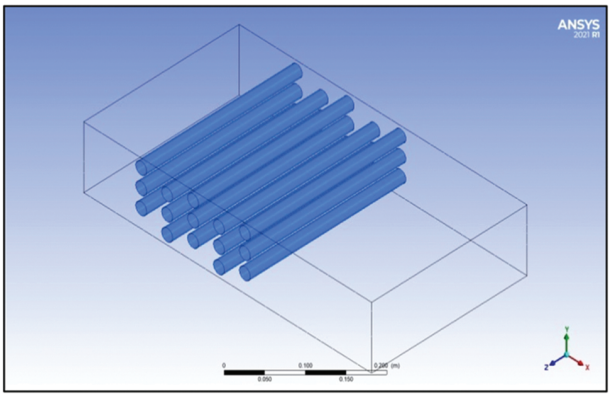

Figure 1d: The three-dimensional distribution of the tube bundle inside the duct with a longitudinal pitch of 45 mm

Momentum (Navier-Stoke):

X- direction (u momentum)

$$u\frac{\partial u}{\partial x}+v\frac{\partial u}{\partial y}+w\frac{\partial u}{\partial z}=-\frac{1}{\rho}\frac{\partial p}{\partial x}+\upsilon\left(\frac{\partial^2 u}{\partial x^2}+\frac{\partial^2 u}{\partial y^2}+\frac{\partial^2 u}{\partial z^2}\right) \tag{3}$$

Y- direction (v momentum)

$$u\frac{\partial v}{\partial x}+v\frac{\partial v}{\partial y}+w\frac{\partial v}{\partial z}=-\frac{1}{\rho}\frac{\partial p}{\partial y}+\upsilon\left(\frac{\partial^2 v}{\partial x^2}+\frac{\partial^2 v}{\partial y^2}+\frac{\partial^2 v}{\partial z^2}\right) \tag{4}$$

Z- direction (w momentum)

$$u\frac{\partial w}{\partial x}+v\frac{\partial w}{\partial y}+w\frac{\partial w}{\partial z}=-\frac{1}{\rho}\frac{\partial p}{\partial z}+\upsilon\left(\frac{\partial^2 w}{\partial x^2}+\frac{\partial^2 w}{\partial y^2}+\frac{\partial^2 w}{\partial z^2}\right) \tag{5}$$

The realizable k-ε turbulence model used in the current simulation along the wall of the tubes. The k-ε model is the straightforward and full form of two equations most frequently employed because it may be applied to complex flows that include swirl, flow separation, and secondary flow because of vortex generation. The essential mathematical statements form the basis of the fluid flow analysis solution. The governing equation is modeled by considering the fluid to be incompressible, single phase, fully developed steady state. The k-ε turbulent model is based on the transport equation for the turbulent kinetic energy (k) and the dissipation rate (ε). The equations that control the computer model can be expressed in the Cartesian coordinates as;

Conservation of mass

$$\frac{\partial \rho}{\partial t}+\nabla.\rho\vec{V}=0 \tag{6}$$

Conservation of momentum

$$\frac{\partial}{\partial t}(\rho\vec{V})+\nabla.\left(\rho\vec{V}\vec{V}\right)=-\nabla P+\nabla.\left(\bar{\bar{\tau}}\right)+\rho\vec{g}+\vec{F} \tag{7}$$

Conservation of energy

$$\frac{\partial}{\partial t}(\rho E)+\nabla.\{\vec{V}+(\rho E+P)\}=\nabla.(\lambda\nabla T) \tag{8}$$

The transport equation for the realizable k-ε model:

Turbulent kinetic energy

$$\frac{\partial}{\partial t}(\rho k)+\frac{\partial}{\partial x_j}\left(\rho k u_j\right)=\frac{\partial}{\partial x_j}\left[\left(\mu+\frac{\mu_t}{\alpha_k}\right)\frac{\partial k}{\partial x_j}\right]+G_k+G_b-\rho\varepsilon-Y_M+S_k \tag{9}$$

Turbulent dissipation rate

$$\frac{\partial}{\partial t}(\rho\varepsilon)+\frac{\partial}{\partial x_j}\left(\rho\varepsilon u_j\right)=\frac{\partial}{\partial x_j}\left[\left(\mu+\frac{\mu_t}{\alpha_\varepsilon}\right)\frac{\partial_\varepsilon}{\partial x_j}\right]+\rho C_1 S_\varepsilon-\rho C_2\frac{\varepsilon^2}{k+\sqrt{\upsilon\varepsilon}}+C_{1\varepsilon}\frac{\varepsilon}{k}C_{3\varepsilon}G_b+S_\varepsilon \tag{10}$$

where, C_1, C_2, $C_{1\varepsilon}$ *and* $C_{3\varepsilon}$ are constants.

2.1 Solution Procedure

A realizable k-ε turbulence sample, calculated at steady-state, implicit formulation, and energy equation is utilized in conjunction with the separable solver in the FLUENT program to tackle this issue. Similar to this, the upwind of the second-order technique is utilized for the density and momentum equation, while a SIMPLE approach is employed for the pressure coupled. In the current

research, The governing equations' accompanying boundary conditions are solved using the Finite Volume Method (FVM) by taking the forced convective flow into account, a three-dimensional (3D) computational model is created listed equations are used to find out the thermal performance of the tube bundle. The following presumptions are taken into account:

a) The fluid flow is assumed in a continuous, steady state and turbulence flow.
b) The velocity is assumed uniform in the inlet.
c) The fluid phase (air) is incompressible.
d) There are no local thermodynamic losses and the effects of radiation are disregarded.
e) At constant temperature, the tube wall was subjected to the no-slip boundary condition.

The following formulas can be used to compute Reynolds number and maximum velocity [25–28]:

$$Re_{max} = \frac{V_{max}.\mathrm{D}}{\upsilon} \tag{11}$$

$$V_{max} = \frac{S_T}{2(S_D - D)} V_i \tag{12}$$

$$V_{max} = \frac{S_T}{S_T - D} V_i \tag{13}$$

The convection heat transfer coefficient is calculated by [29]:

$$\bar{h} = \overline{Nu}\frac{K}{D} \tag{14}$$

The log-mean temperature can be computed from [30]:

$$\Delta T_{lm} = \frac{\left(T_{S,a} - T_i\right) - \left(T_{S,a} - T_o\right)}{Ln\left[\frac{\left(T_{S,a} - T_i\right)}{T_{S,a} - T_o}\right]} \tag{15}$$

The exit temperature can be valued from [31]:

$$\left(T_{S,a} - T_o\right) = \left(T_{S,a} - T_i\right) \exp\left[-\frac{\pi D L \bar{h}}{\rho V_i N_T S_T C_P}\right] \tag{16}$$

The total heat transfer rate may be calculated using the equation shown below [31]:

$$Q = N(\pi D L \bar{h} \Delta T_{lm}) \tag{17}$$

2.2 The Mesh and Boundary Conditions

Using cells that are quadrilateral and tetrahedral, the mesh for this issue has been constructed for the domain by keeping the mesh quality at 0.83, and the skewness was 0.66. The non-uniform mesh is produced to enable a more accurate fluid flow. The model contains a fine mesh element with refining the mesh along the tube wall to allow for greater resolution of heat transmission. To fully capture the boundary layer generation over the cylinder, a total of 15 prism layer elements were produced with an initial height of 0.08 mm and a growth rate of 1.1, which is noticeably high. Figs. 2a and 2b separately show the mesh distribution and the arrangement of the mesh around the tubes. The initial conditions in terms of temperature, pressure, and speed of the test section were set to zero. The ambient temperature and pressure were set at 300 K and 101 Kpa, respectively. The inlet, outlet, and tube walls have been designated as the problem's boundary locations. The inlet receives air at a temperature of 300 K and velocity applied of 0.9, 1.1, 1.4, and 1.7 m/s. The outlet pressure was set the same as the

ambient pressure. The heat flux applied on the wall of the tube changed from 1551, 6205, 10858, and 15512 W/m^2 respectively. Table 2 displays the air characteristics that were utilized in the inlet section of the model.

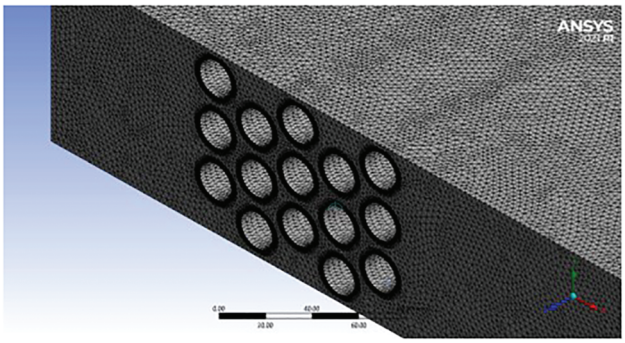

Figure 2a: Shows the mesh distribution

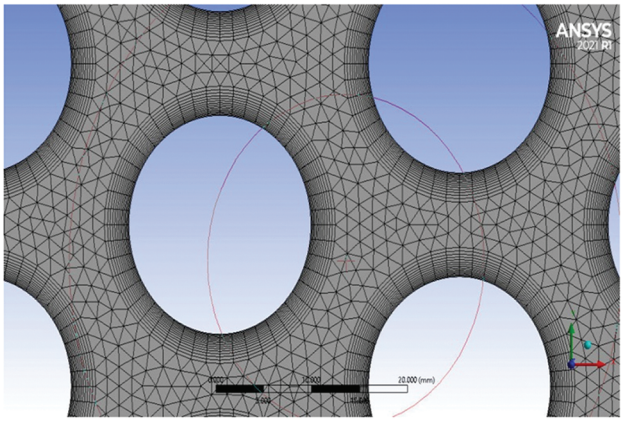

Figure 2b: Shows the arrangement of the mesh around the tubes

Table 2: Properties of air used in the inlet domain

No.	Air properties	Quantity
1	The density of air-ρ (Kg/m^3)	1.225
2	The viscosity-ν (Kg/m.s)	1.784×10^{-5}
3	The thermal conductivity of air-k (W/m.K)	0.0242
4	The specific heat of air-Cp (J/Kg. K)	1006.43
5	Prandtl number-Pr	0.707
6	The outside air temperature-T∞ (K)	300

The essential check must be carried out for the minimum number of cells required for grid independence in the event of the numerical simulation grid independence is indispensable for the precision, repeatability, and validity of the numerical methods. Consequently, the four various grid systems comprising 1406920, 2228046, 5908868, and 12565385 of the number of cells were selected.

Fig. 3 demonstrates how the grid is dependent on the average Nu for the Re of 10000. The graph shows a little change in the comparable Nu from 5.9 to 12.6 million cells, however, the change after that is not noticeable. Additionally, with the nominal change in the average Nu, the calculation time for the numerical simulation increases significantly. Table 3 provides information about the computational grid utilized in the current numerical simulation. For each grid system, the Nu was analyzed. It has been determined that the variation in the Nu for the most recent grid size, which included 12565385 cells, is not substantial and is on the order of 0.5%. Therefore, a cell size with 5908868 numbers of nodes was chosen for the numerical simulation by taking into account the fluctuation in the Nu as well as the calculation time requirement.

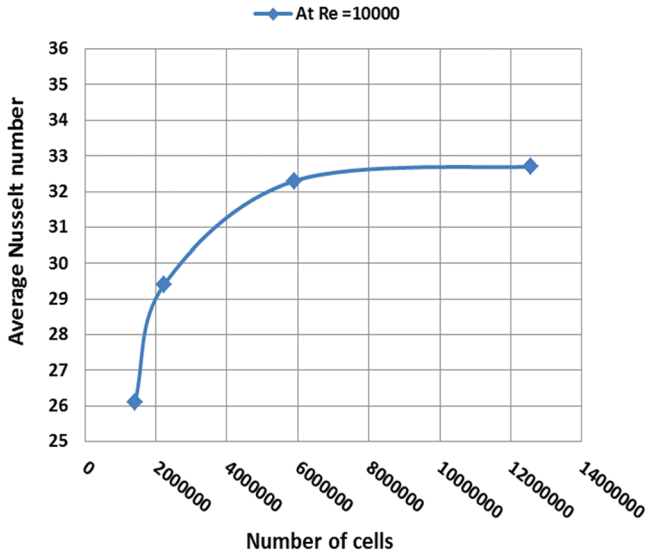

Figure 3: Grid independence

Table 3: Mesh independence analysis at Re = 10000

Grads Nu	Cell size	Number of cells	Average nusselt number
1	4 mm	1406920	26.1
2	3 mm	2228046	29.4
3	2 mm	5908868	32.3
4	1 mm	12565385	32.7

3 The Validation

A few of the previously published benchmark issues were compared to the numerical model. It was projected how fluid flowing and heat transmission would occur over a line in staggered orbicular tubes subject to varying wall temperatures and heat flow. Using earlier research to compare the Nusselt number for the completely formed area amidst tubes with varied wall temperatures compares the results of the current study to earlier research by Mangrulkar et al. [7] for an array of oval tubes with an in-line arrangement. The tube diameter is 22.44 mm and the tube length is 22 mm. The longitudinal and transverse pitch ratios of 1.5 mm and 1.25 mm, respectively. The range of the Reynold number

is 12000 to 24000. It enables us to see that the current results and the numerical results show perfect agreement with Mangrulkar et al. [7] for the average Circumference of the Nusselt number distribution. Fig. 4 showed compare between the average Nusselt numbers at the range of heat flux 15512 W/m^2.

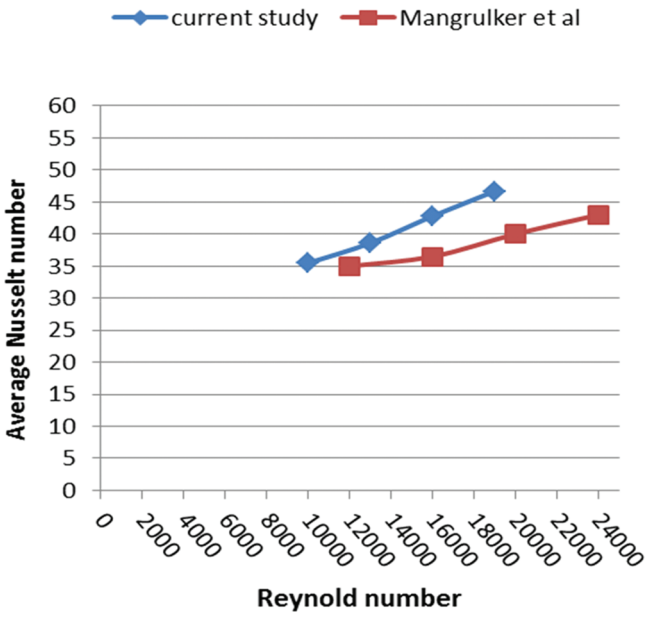

Figure 4: Average Nusselt number change with Reynold number at heat flux 10858 W/m^2

4 The Results and Discussion

A numerical simulation of a 3D tube bundle was performed. Using the FLUENT program can predict the average Nusselt number values for heat fluxes that vary between 1551 and 15512 W/m^2. The effect of changing the longitudinal spacing by changing the heat flux was also studied as shown in Fig. 5. The figure demonstrates that a raise in the heat flux on the tube's surface causes a rise in the average Nusselt number at Reynold number 10000. In addition, the influence of air velocity on the Nusselt number was investigated. The average Nusselt number changes with heat flux at various input air velocities.

The best model was chosen for further testing. The model with a longitudinal pitch of 25 mm is the best in terms of the best heat transfer and the highest Nusselt number. The tests are to be conducted to discuss the change of heat transfer of the tube bundle when changing the heat flux at different Reynolds number values. Table 4 indicates the average Nu for the numerical simulation for various Re. Figs. 6 to 9 show provide the average Nusselt number changes with the Reynolds number at different heat fluxes. These plates demonstrate that when the Reynolds Number and surface heat flux increase, the average Nusselt number increases.

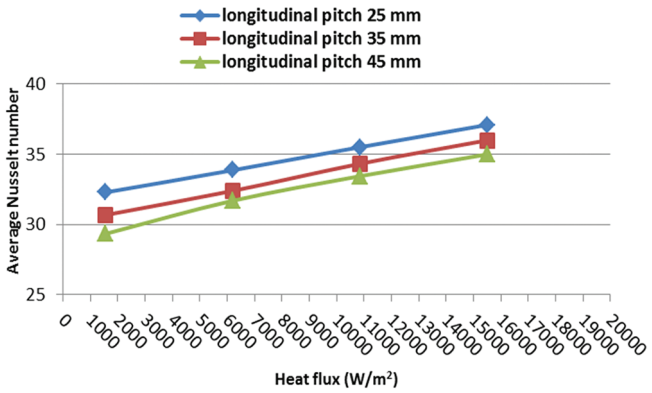

Figure 5: Nusselt number varies with changing heat flux at Reynold number 10000

Table 4: Indicates the average Nu for the numerical simulation at different Re

Re	Nu. At heat flux 1551 (W/m^2)	Nu. At heat flux 6205 (W/m^2)	Nu. At heat flux 10858 (W/m^2)	Nu. At heat flux 15512 (W/m^2)	Mangrulkar et al. Nusselt Nu
10000	32.29	33.87	35.5	37.1	35
13000	35.7	36.6	38.6	40	37
16000	40.4	41.5	42.8	44.1	40
19000	44.6	45.5	46.7	48	42

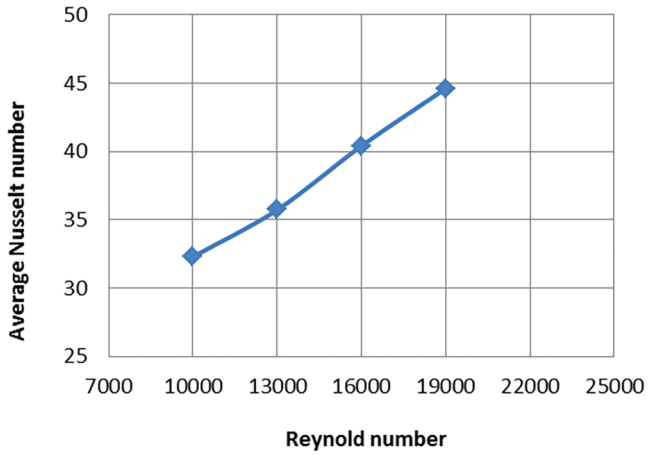

Figure 6: Nusselt number varies with changing Reynolds numbers at longitudinal pitch 25 mm and heat flux 1551 W/m^2

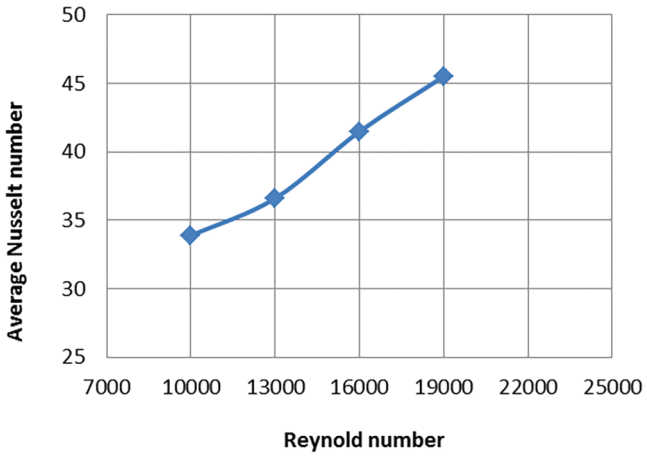

Figure 7: Nusselt number varies with changing Reynolds numbers at longitudinal pitch 25 mm and heat flux 6205 W/m^2

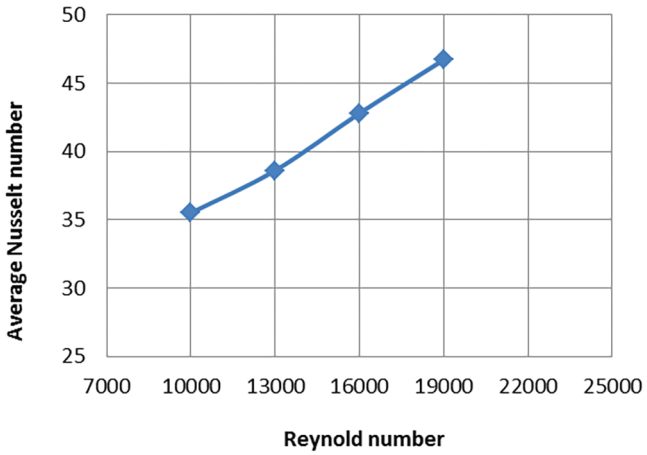

Figure 8: Nusselt number varies with changing Reynolds numbers at longitudinal pitch 25 mm and heat flux 10858 W/m^2

Fig. 10 shows the turbulent kinetic energy and flow streamlines for chosen cases with Re = 10,000: (a and b) tube bundle with longitudinal pitch $S_L = 25$ mm, (c and d) tube bundle with longitudinal pitch $S_L = 35$ mm, (e and f) tube bundle with longitudinal pitch $S_L = 45$ mm. For each of the cases that are shown, the TKE intensity progressively increases in the direction of the stream before peaking just downstream of the last row. The effect of longitudinal pitch on the TKE can be observed when comparing Figs. 10b, 10d, and 10f. It can be seen that the turbulent kinetic energy is greater in the tube bundles with a longitudinal pitch of 25 mm than the tube bundle in which the longitudinal pitch is 35 and 45 mm, respectively, because the lower longitudinal pitch leads to an increase in the friction factor and thus an increase in the turbulent kinetic energy values. The following is a description of the flow topology of the case (a and b). The first row of tubes is being struck by the upstream flow, causing stagnation patterns in front of the tubes. The flow streamlines then move near the tube walls. Following that, a vortex area is created behind the tubes and the separation is noticeable due to the curvature of the tube circumference. At these airflow conditions, and when the longitudinal pitch is

large compared to the transverse pitch, there is a delay at the beginning of the flow separation, which leads to a change in the structure of the flow. Therefore, we notice a deviation of the flow over the pipes from the line of symmetry.

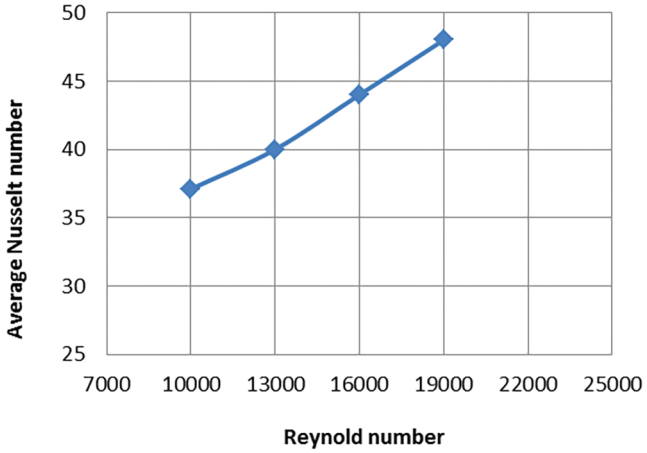

Figure 9: Nusselt number varies with changing Reynolds numbers at longitudinal pitch 25 mm and heat flux 15512 W/m^2

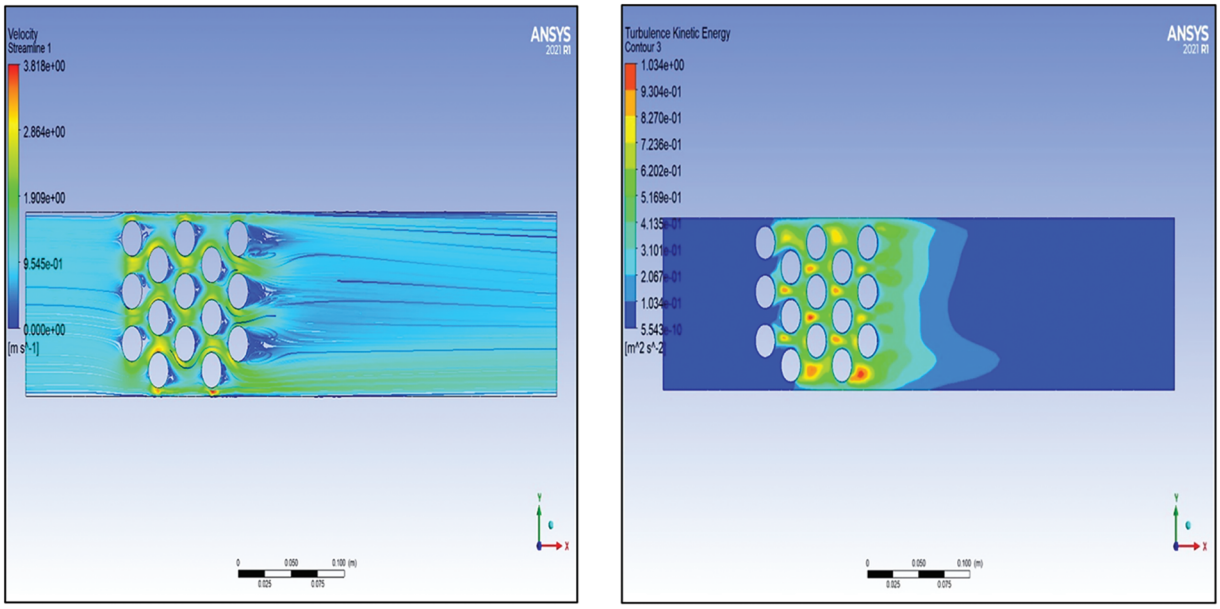

(a) **(b)**

Figure 10: (Continued)

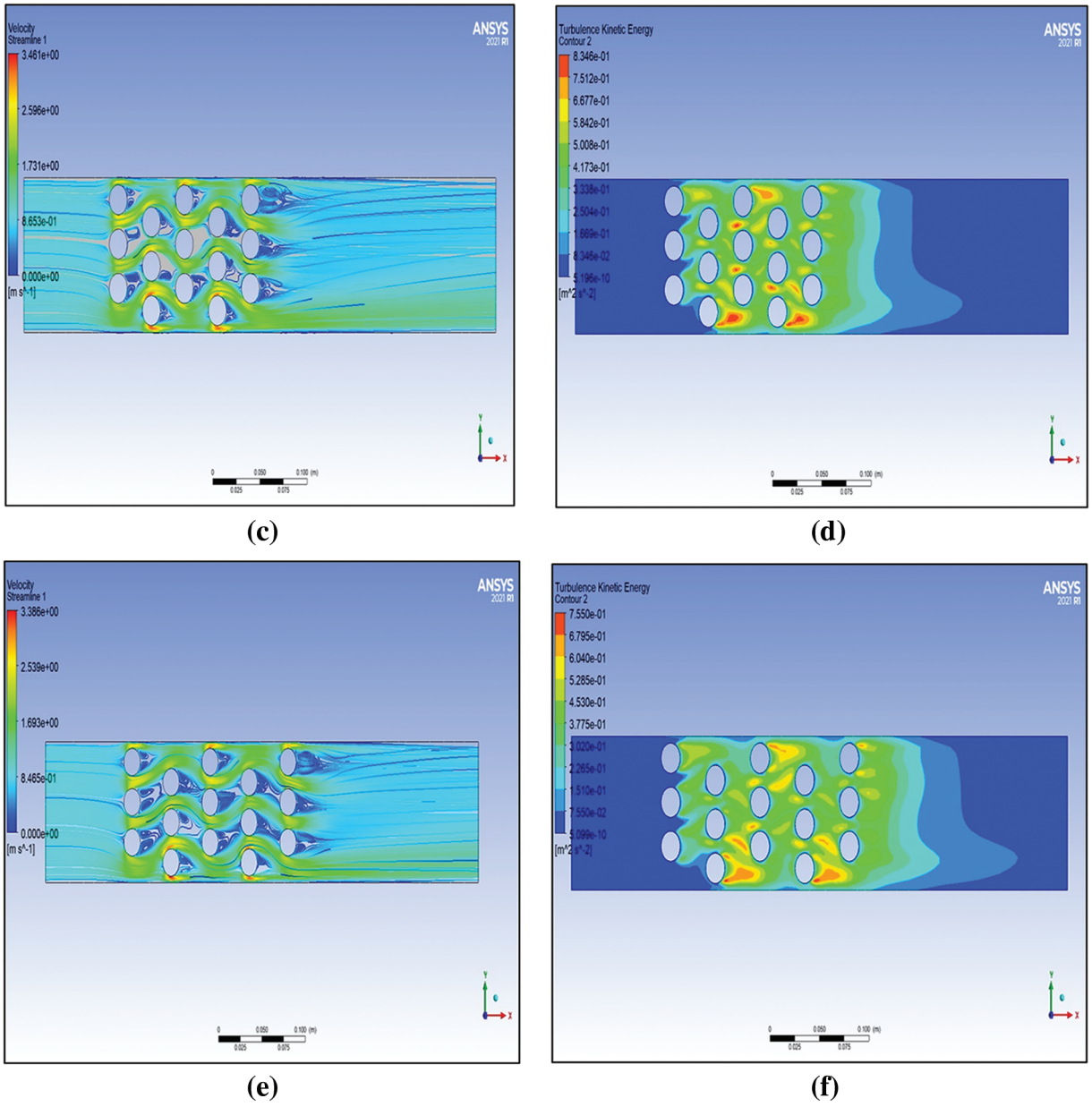

Figure 10: Streamlines and Turbulent Kinetic Energy across the tube banks: (a,b) transverse pitch ST 28 mm, longitudinal pitch S_L= 25 mm, velocity 0.9 m/s, and heat flux 6205 W/m^2. (c,d) Transverse pitch ST 28 mm, longitudinal pitch S_L = 35 mm, velocity 0.9 m/s, and heat flux 6205 W/m^2. (e-f) Transverse pitch ST 28 mm, longitudinal pitch S_L = 45 mm, velocity 0.9 m/s, and heat flux 6205 W/m^2

5 Conclusions

Staggered tube bundles were used in the three-dimensional computational fluid dynamics simulations. The results from the developed model were examined under various operational situations using

ANSYS FLUENT. Heat flux and longitudinal pitch effects were investigated. Following are some of the major facets of the current study:

- The tube bundle with a longitudinal pitch of 25 mm provides greater heat transmission characteristics when compared to the tube bundle with a longitudinal pitch of 35 and 45 mm.
- In the tube bundle with a longitudinal pitch of 25 mm, the results indicate that with the heat flux of the tube bundle walls increases by 75% the average Nusselt number increases by 5% when the velocity of air remains constant.
- When heat flux increased by 30% the average Nusselt number increased by 2.7% at constant air velocity
- The average Nusselt number increases by 25% if the Reynolds number is increased from 10,000 to 19,000 when the heat flux is held constant in a tube bundle with a longitudinal pitch of 25 mm.

Acknowledgement: The authors gratefully admit the scientific backing of the Division of Mechanical Engineering at Mustansiriyah University (www.uomustansiriyah.edu.iq), College of Engineering in Iraq.

Funding Statement: The authors received no specific funding for this study.

Author Contributions: The authors confirm contributions to the paper as follows: study conception and design: Husam Rashid Hudear, Saad Najeeb Shehab; data collection: Saad Najeeb Shehab; analysis and interpretation of results: Husam Rashid Hudear, Saad Najeeb Shehab; draft manuscript preparation: Husam Rashid Hudear. Saad Najeeb Shehab. All authors reviewed the results and approved the final version of the manuscript.

Availability of Data and Materials: The data used to support the findings of this study are included within the article.

Conflicts of Interest: The authors declare that they have no conflicts of interest to report regarding the present study.

References

1. Li, X., Wu, X., He, S. (2014). Numerical investigation of the turbulent cross flow and heat transfer in a wall-bounded tube bundle. *International Journal of Thermal Sciences, 75(3),* 127–139. https://doi.org/10.1016/j.ijthermalsci.2013.08.001
2. Sahamifar, S., Kowsary, F., Mazlaghani, M. H. (2019). Generalized optimization of cross-flow staggered tube banks using a subscale model. *International Communications in Heat and Mass Transfer, 105(5),* 46–57. https://doi.org/10.1016/j.icheatmasstransfer.2019.03.004
3. Ramezanpour, A., Shirvani, H., Rahmani, R., Mirzaee, I. (2005). HT2005-72532. Three-dimensional numerical modeling of the staggered tube bundles turbulent cross FLOW in the duct. Online, Available: http://www.asme.org/about-asme/terms-of-use
4. Jang, J. Y., Yang, J. Y. (1998). Experimental and 3-D numerical analysis of the thermal-hydraulic characteristics of elliptic finned-tube heat exchangers. *Heat Transfer Engineering, 19(4),* 55–67. https://doi.org/10.1080/01457639808939936

5. Ibrahim, T. A., Gomaa, A. (2009). Thermal performance criteria of the elliptic tube bundle in cross flow. *International Journal of Thermal Sciences, 48(11),* 2148–2158. https://doi.org/10.1016/j.ijthermalsci.2009.03.011
6. Tahseen, T. A., Ishak, M., Rahman, M. M. (2011). A numerical study of forced convection heat transfer for staggered tube banks in cross-flow. *1ST International Conference in Mechanical Engineering Research (ICMER)*, Pahang, Malaysia.
7. Mangrulkar, C. K., Dhoble, A. S., Deshmukh, A. R., Mandavgane, S. A. (2017). Numerical investigation of heat transfer and friction factor characteristics from in-line CAM-shaped tube bank in cross flow. *Applied Thermal Engineering, 11,* 521–538. https://doi.org/10.1016/j.applthermaleng.2016.08.174
8. Saraireh, M. A., Al-Saraireh, F., Alrwashdeh, S., Saraireh, M. A., Alsaraireh, F. M. et al. (2017). Alrwashdeh, Investigation of heat transfer for staggered and in-line tubes. *International Journal of Mechanical Engineering and Technology, 8(11),* 476–483. http://www.iaeme.com/IJMET/index.asp476editor
9. Refaey, H. A., Sultan, A. M., Moawad, M., Abdelrahman, M. A. (2019). Numerical investigations of the convective heat transfer from turbulent flow over staggered tube bank. *Journal of the Institution of Engineers (India): Series C, 100(6),* 983–993. https://doi.org/10.1007/s40032-018-0493-z
10. Petinrin, M. O., Towoju, O. A., Ajiboye, S. (2019). Numerical study of the effect of changing tube pitches on heat and flow characteristics from tube bundles in cross flow. *Journal of Engineering Sciences, 6(2).* https://doi.org/10.21272/jes.2019.6(2)
11. Deeb, R., Sidenkov, D. V. (2021). Numerical analysis of heat transfer and fluid flow around circular and non-circular tubes. *Journal of Physics: Conference Series, 2088(1),* 012008. https://doi.org/10.1088/1742-6596/2088/1/012008
12. Tassone, A., Meeusen, J., Serafini, A., Caruso, G. (2021). On the simulation of turbulent heat transfer for low-Pr fluid cross-flow in tube banks. *SSRN Electronic Journal, 4(4),* 2. https://doi.org/10.2139/ssrn.3969848
13. Kotšmíd, S., Brodnianská, Z. (2021). Determination of the reference temperature for a convective heat transfer coefficient in a heated tube bank. *Applied Sciences, 11(22),* 10564. https://doi.org/10.3390/app112210564
14. Ariansyah, M. N., Diana, L., Satrio, D. (2022). Numerical study the effect of gap ratio on flow characteristics and heat transfer in staggered tube banks. *IOP Conference Series: Earth and Environmental Science, 972(1),* 012065. https://doi.org/10.1088/1755-1315/972/1/012065
15. Wang, Y. Q., Jackson, P., Phaneuf, T. J. (2006). Turbulent flow through a staggered tube bank. *Journal of Thermophysics and Heat Transfer, 20(4),* 738–747. https://doi.org/10.2514/1.18973
16. Bender, A., Meier, A. M., Vaz, M., Zdanski, P. S. B. (2018). A numerical study of forced convection in a new trapezoidal tube bank arrangement. *International Communications in Heat and Mass Transfer, 91,* 117–124. https://doi.org/10.1016/j.icheatmasstransfer.2017.12.007
17. Mu, L., Wang, S., Zhai, Z., Shang, Y., Zhao, C. et al. (2020). Unsteady CFD simulation on ash particle deposition and removal characteristics in tube banks: Focusing on particle diameter, flow velocity, and temperature. *Journal of the Energy Institute, 93(4),* 1481–1494. https://doi.org/10.1016/j.joei.2020.01.010
18. Zhang, L. Z., Ouyang, Y. W., Zhang, Z. G., Wang, S. F. (2015). Oblique fluid flow and convective heat transfer across a tube bank under uniform wall heat flux boundary conditions. *International Journal of Heat and Mass Transfer, 91,* 1259–1272. https://doi.org/10.1016/j.ijheatmasstransfer.2015.08.062
19. Wang, Y. Q., Jackson, P. L. (2010). Turbulence modeling was applied to flow through a staggered tube bundle. *Journal of Thermo Physics and Heat Transfer, 24(3),* 534–543. https://doi.org/10.2514/1.44356
20. Zheng, Z., Yang, W., Cai, Y., Wang, Q., Zeng, G. (2020). Dynamic simulation on ash deposition and heat transfer behavior on a staggered tube bundle under high-temperature conditions. *Energy, 190(5),* 116390. https://doi.org/10.1016/j.energy.2019.116390

21. Khan, M. S., Zou, R., Yu, A. (2021). Computational simulation of air-side heat transfer and pressure drop performance in staggered mannered twisted oval tube bundle operating in cross flow. *International Journal of Thermal Sciences, 161,* 106748. https://doi.org/10.1016/j.ijthermalsci.2020.106748
22. Jodaei, A., Zamzamian, K. (2017). A Study about performance evaluation criteria of tube banks with various shapes and arrangements using numerical simulation. *Journal of Pressure Vessel Technology, Transactions of the ASME, 139(5),* 1–9. https://doi.org/10.1115/1.4037637
23. Omar, H., Alfarawi, S., El-sawi, A., Zeo, M. (2021). Numerical simulation of cross flow in in-line square tube array to estimate the convective heat transfer coefficient. *American Journal of Energy Research, 9(2),* 84–91. https://doi.org/10.12691/ajer-9-2-2
24. Shameran, J. S. (2019). Numerical study of the effect of changing tube pitches on heat and flow characteristics from tube bundles in cross flow. *Journal of Engineering Sciences, 2,* e1–e10. https://doi.org/10.21272/jes.2019.6(2).e1
25. Deeb, R., Sidenkov, D. V. (2020). Investigation of flow characteristics for drop-shaped tubes bundle using ansys package. *2020 5th International Conference on Information Technologies in Engineering Education (Inforino)*. Moscow, Russia. https://doi.org/10.1109/Inforino48376.2020.9111775
26. Zdravistch, F., Fletcher, C. A., Behnia, M. (1995). Numerical laminar and turbulent fluid flow and heat transfer predictions in tube banks. *International Journal of Numerical Methods for Heat & Fluid Flow, 5(8),* 717–733. https://doi.org/10.1108/EUM0000000004086
27. Moosavi, A., Ljung, A., Lundström, T. S. (2023). A comparative study on thermo-fluid characteristics of free and wall-bounded cross-flow heat exchangers. *Thermal Science and Engineering Progress, 40,* 101746. https://doi.org/10.1016/j.tsep.2023.101746
28. Karali, M. A., Awadh, B., Bin, A. S., Abdelmohimen, M. A. H., Attia, E. et al. (2023). Case studies in thermal engineering effect of surfaces roughness of a staggered tube bank in cross flow with air on heat transfer and pressure drop. *Case Studies in Thermal Engineering,* 102779. https://doi.org/10.1016/j.csite.2023.102779
29. Nemati, H., Samivand, S. (2016). Numerical study of flow over annular elliptical finned tube heat exchangers. *Arabian Journal for Science and Engineering, 41(11),* 4625–4634. https://doi.org/10.1007/s13369-016-2226-z
30. Utomo, B., Widodo, K., Hanifah, S. D. (2017). Numerical analysis on the effect of longitudinal and transversal pitch ratio to the flow and heat transfer characteristic of staggered elliptical tubes-bank. *AIP Conference Proceedings, 1778,* 030020. https://doi.org/10.1063/1.4965754
31. Khan, W. A., Culham, J. R., Yovanovich, M. M. (2006). Analytical model for convection heat transfer from tube banks. *Journal of Thermophysics and Heat Transfer, 20(4)*. https://doi.org/10.2514/1.15453